Boundary effects on the resonant coupling of the excitation modes of semiconductor quantum wells

1999 J. Phys.: Condens. Matter 11 4557

(http://iopscience.iop.org/0953-8984/11/23/309)

J. Phys.: Condens. Matter **11** (1999) 4557–4574. Printed in the UK PII: S0953-8984(99)98509-0

Boundary effects on the resonant coupling of the excitation modes of semiconductor quantum wells

Q Guo, Y P Feng, H C Poon and C K Ong

Department of Physics, National University of Singapore, Kent Ridge, Singapore 119260

Received 20 October 1998, in final form 26 March 1999

Abstract. An alternative approach based on the invariant imbedding method and the random phase approximation is used to study the excitation spectra of both neutral and parabolic quantum wells. Compared to other methods, this approach is efficient and leads to more stable solutions. It also provides a convenient way for studying boundary effects. The calculated excitation spectra for both types of quantum well agree well with experimental observations and previous calculations. The effects of the boundary condition on the excitation spectra were extensively studied. It was found that the positions and relative strengths of resonant peaks are sensitive to the boundary condition. The evolution of some of the resonant peaks can be attributed to the coupling between collective plasma modes and the intersubband transitions.

1. Introduction

With modern crystal growth techniques, such as molecular beam epitaxy (MBE) and metal organic vapour deposition (MOCVD), it is possible to grow high quality $Ga_{1-x}Al_xAs$ quantum well structures, and by controlling the Al composition, x, arbitrary shape for the conduction band minimum energy, E_c, can be obtained along the growth direction [1, 2]. When E_c is parabolic inside the quantum well region and linear outside, the quantum well is referred to as a neutral quantum well (NQW). By contrast, if E_c is parabolic everywhere, the structure is called a parabolic quantum well (PQW) (see figure 1). The study of excitation modes in those structures has received considerable attention in recent years [3–10] due to the significant roles these excitation modes play in the transport and optical properties of these structures. Two types of surface plasma modes [11], 2D-like surface plasmon and bulklike plasmon, have been observed in the far-infrared (FIR) transmission spectra of the parabolic quantum well [4]. Yuh *et al* [12] found that the surface plasmon modes are particularly sensitive to the surface potentials. The effect of surfaces on the bulklike plasmon modes in metallic films was theoretically investigated [13]. Theoretical calculations on semiconductor quantum wells showed that the excitation spectra of neutral quantum wells are quite different from those of PQWs [8–10]. However, there have been some ambiguities in the identification of the resonant peaks in the excitation spectra of NQWs. Most of the previous calculations on NQWs were carried out by imposing the hard-wall boundary condition [8, 9]. Two infinite barriers were imposed on the boundaries to force the wave functions to vanish at the boundaries (see figure 1(b)). Recently, Schaich and Dobson [10] studied the excitation spectra in NQWs using a soft-wall boundary condition (see section 4) and demonstrated that the boundary condition significantly affects the excitation spectra. In structures such as a resonant tunnelling barrier (RTB) diodes, the barriers act as boundaries and provide confinement of charge carriers outside

0953-8984/99/234557+18$19.50

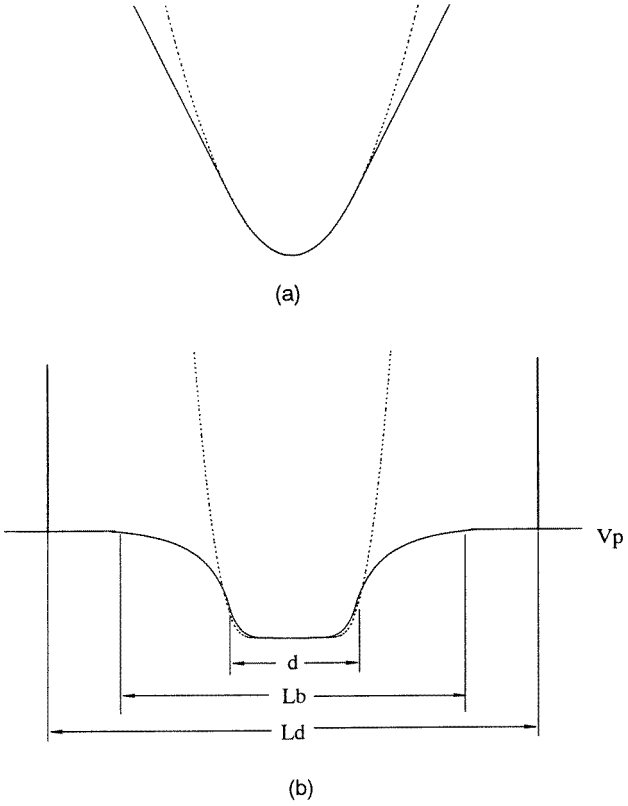

Figure 1. (a) Schematic view of the conduction energy E_c of the neutral quantum well (solid curve) and parabolic quantum well (dashed curve). (b) The self-consistent potential energy of the neutral quantum well (solid curve) and parabolic quantum well (dashed curve) with width $d = 8.8$ au* and density $n^+ = 0.0275$ au*. The two solid vertical lines show the hard-wall boundary barriers of the neutral quantum well. L_b represents the distance between the hard-wall boundaries used in the calculation of the self-consistent electronic structure. L_d stands for the distance between the hard-wall boundaries used in the calculation of the excitation spectra.

the quantum wells. Studies have shown that the characteristics of RTB diodes can be improved dramatically by choosing appropriate barrier materials [12]. The structures of such systems are remarkably similar to quantum wells with hard-wall boundaries.

In the calculation of excitation modes, the ground state electronic structure of quantum wells is usually obtained by employing the local density approximation (LDA). Their excitation spectra are generally evaluated using the random phase approximation (RPA). In most of these calculations, the self-consistent electronic structure is found by numerical integration of the one-dimensional Schrödinger equation. As for the free response function, two different methods have been employed to evaluate the Green function appearing in the free response function. In the first method [15, 16], the Green function is obtained by summing over the energy eigenstates. For neutral quantum wells this sum becomes an integral over the energy continuum above the escape threshold (the plateau value of the total potential energy outside the well). This method is time consuming because the sum over the eigenstates converges slowly. In the second method, the sum of the eigenstates is first converted to a Green function which is expressed in terms of a product of 'left' and 'right' moving solutions of the one-dimensional

Schrödinger equation [17]. The second method is obviously more efficient than the first one. However, for regions where the solution is exponentially increasing or decreasing, it may cause numerical instability if the step size is not sufficiently reduced. For three-dimensional wells, the problem is potentially more serious. In such cases, round-off errors would destroy the linear independence of intermediate solutions for evanescent channels and cause numerical difficulties. In the present study of excitation spectra in NQWs and PQWs, we adopt an alternative approach based on the invariant imbedding method for the calculation of the self-consistent electronic structure [18]. In this approach, the Green function is calculated from the reaction matrix in the complex energy plane. The free response function is calculated by integrating the Green function over a contour in the complex energy plane. Because the integrand is smooth, only a few integration points are required. Therefore, the method provides a more efficient and stable scheme for the calculation of excitation spectra of quantum wells. It has been shown that the calculated ground state properties are in good agreement with available experimental data and previous theoretical results. Furthermore, the boundary condition is naturally embedded in the calculation of reaction matrix and its effects on the excitation modes can be readily studied using this approach. Calculation using a one-dimensional potential is presented in the following. The formalism, however, can be easily extended to three-dimensional structures. The invariant imbedding method has been used in the study of electronic structures of jellium surfaces [19], atom–molecule scattering [20] and reflection high energy electron diffraction (RHEED) [21] and it has been proved to be a successful and efficient method.

In this study, the method is used first to calculate the excitation spectra of the PQW. It is then extended to the study of the excitation spectra of the NQW. The effects of boundary condition on the excitation modes are investigated. In the following section, we will describe the theory underlying the approach. The numerical method will be discussed in section 3. In section 4, the calculated results pertaining to the excitation spectra of both the NQW and PQW will be presented. The evolution of the resonant peaks in the excitation spectra of the NQW due to the change of boundary condition and their physical origins will be discussed. Finally we will summarize our results in section 5.

2. Theory

For $Ga_{1-x}Al_xAs$ quantum wells, the effective mass, m^*, is about 0.069 m_0 and the dielectric constant, ε_0, is around 13.0. The effective Bohr radius, a_0, is around 100 Å, which is much larger than the lattice constant. We can therefore ignore the crystalline structure of the host, and assume that the spatially varying energy $E_c(z)$ due to the varying composition along the quantum well growth direction z takes the role of an external potential energy function $V_{bare}(z)$ based on the envelope function approximation. The electron is then confined in the z direction by the potential $V_{bare}(z)$ plus its own self-consistent electrostatic field with effective mass m^*, but free to move in the x and y directions parallel to the epitaxial layers. In the $Ga_{1-x}Al_xAs$ system, the spatially varying Al content gives rise to a spatial variation of the effective mass and of the semiconductor dielectric constant of up to 10% in experiment [4], which will be ignored in the present work. Within this approximation, the self-consistent Kohn–Sham eigenfunction of quantum wells may be written as

$$\Psi_J \equiv \Psi_{k_\parallel, j}(\vec{r}) = \frac{1}{3\pi} \exp(\vec{k} \cdot \vec{\rho}) \psi_j(z) \tag{1}$$

with eigenenergy

$$E_J \equiv E(\vec{k}_\parallel, j) = \varepsilon_j + \tfrac{1}{2}k_\parallel^2 \tag{2}$$

where $\vec{r}$ is a position vector, and $\vec{\rho}$ and z are the projections of $\vec{r}$ parallel and normal to the well respectively, while $\vec{k}_\parallel$ is the projection of $\vec{k}$ parallel to the well. ε_j is the eigenenergy of the one-dimensional Schrödinger equation with self-consistent potential, and $\psi_j(z)$ is the corresponding eigenfunction.

For independent electrons moving in the self-consistent ground state potential, the density response δn_f to a small time-dependent external perturbation,

$$\delta v = v_x(z, q_\parallel) \exp[\mathrm{i}(\vec{q}_\parallel \cdot \vec{r} - \omega t)] \tag{3}$$

can be written as

$$\delta n_f(z, q_\parallel, \omega) = \int \mathrm{d}z' \Pi^0(q_\parallel, z, z', \omega) v_x(z', q_\parallel) \tag{4}$$

where the free response function is given by

$$\Pi^0(q_\parallel, z, z', \omega) = \frac{1}{2\pi^2} \sum_i^{occ} \psi_i(z)\psi_i(z') \int \mathrm{d}\vec{k}_\parallel \left\{ \sum_j \frac{\psi_j(z)\psi_j(z')}{\varepsilon^+ - \varepsilon_j} + \sum_j \frac{\psi_j(z)\psi_j(z')}{\varepsilon^- - \varepsilon_j} \right\} \tag{5}$$

where

$$\varepsilon^\pm = \varepsilon_i \pm (\omega + \vec{k}_\parallel \cdot \vec{q}_\parallel) - \tfrac{1}{2} q_\parallel^2. \tag{6}$$

It is noted that the two terms in the braces of equation (5) are just the Green functions for the one-dimensional Schrödinger equation with energy of ε^+ and ε^- respectively. Therefore the free response function can be written as

$$\Pi^0(q_\parallel, z, z', \omega) = \frac{1}{2\pi^2} \sum_i^{acc} \psi_i(z)\psi_i(z') \int \mathrm{d}\vec{k}_\parallel [G^+(z, z', \varepsilon^+) + G^+(z, z', \varepsilon^-)]. \tag{7}$$

In most of the previous works, the free response functions were numerically obtained by two different methods. One method is based on equation (5), where the sums over intermediate one-dimensional eigenstates j are carried out directly. This sum becomes an integral over ε^+ (ε^-) above the escape threshold. The second method makes use of equation (7). The Green function is evaluated in terms of 'left moving' and 'right moving' solutions at energy ε^+ and ε^- respectively of the one-dimensional Schrödinger equation. However, the first method is time consuming and the second method may cause numerical instability in some cases as discussed above. In the following, we use an alternative approach based on the invariant imbedding method for the calculation of dynamic response function of a quantum well in the RPA.

It can be proved that the Green function at a certain plane of the quantum well can be written as

$$G(z, z', \varepsilon) = -\frac{\mathrm{i}}{k_z} D(z, z', \varepsilon) \tag{8}$$

where

$$k_z = \sqrt{2\varepsilon} \tag{9}$$

and $D(z, z', \varepsilon)$, the propagation function, is the total amplitude of the scattered plane wave at z' if there are two plane waves starting at z with energy ε and directions k_z^+ and k_z^- respectively. We will discuss the form of $D(z, z', \varepsilon)$ in the case of $z' > z$. Assuming the region to the right of z' is free space, the sum of amplitudes of scattered plane waves at z' is

$$D'(z, z', \varepsilon) = \frac{M^{++}(1 + M_2(z))}{1 - M_2(z)M^{-+}} \tag{10}$$

where $M_2(z)$ is the reflection matrix from the potential region $(-\infty, z)$; M^{++} and M^{-+} are the transmission and reflection matrices respectively for a wave moving along the $+z$ direction due

to the potential slab between z and z' (see figure 2). Adding the potential to the right of z', the total amplitude of scattered plane wave becomes

$$D(z, z', \varepsilon) = \frac{D(1 + M_1(z'))}{1 - M_1(z')M_2(z')} \tag{11}$$

where $M_1(z')$ and $M_2(z')$ are reflection matrices from the potential region (z', ∞) and $(-\infty, z')$ respectively (see figure 2). Substituting equation (10) into equation (11), we obtain

$$D(z, z', \varepsilon) = \frac{(1 + M_2(z))M^{++}(1 + M_1(z'))}{(1 - M_1(z)M^{-+})(1 - M_1(z')M_2(z'))} \qquad (z' > z). \tag{12}$$

Similarly, we have

$$D(z, z', \varepsilon) = \frac{(1 + M_2(z))M^{--}(1 + M_2(z'))}{(1 - M_1(z)M^{+-})(1 - M_1(z')M_2(z'))} \qquad (z' < z). \tag{13}$$

where $M_1(z)$ is the reflection matrix from the potential region with (z, ∞); M^{--} and M^{+-} are the transmission and reflection matrices respectively for a wave moving along the $-z$ direction due to the potential slab between z and z'.

To obtain the transmission and reflection matrices of a slab, we first divide a slab into thin slices within which the potential can be considered to be approximately constant. Consider an incident plane wave with wave vector k_z propagating through a slice of thickness h with

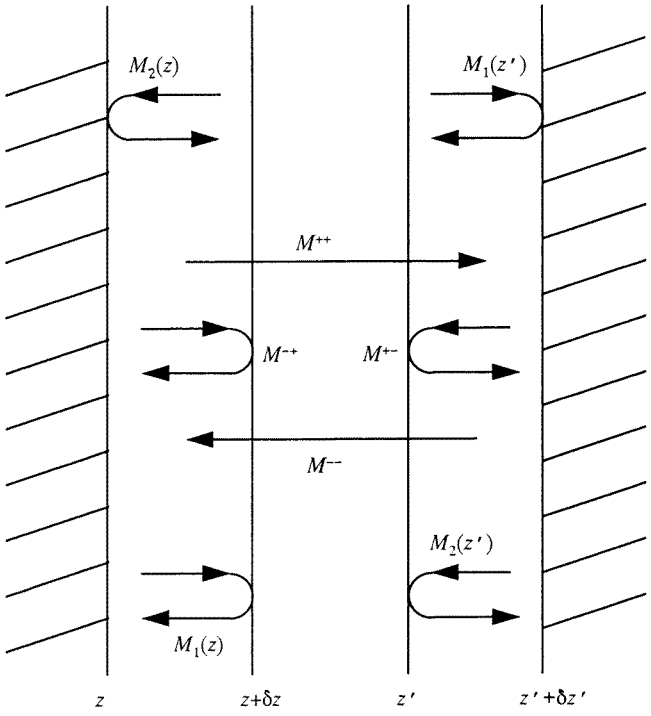

Figure 2. Scattering matrices: $M_1(z)$ and $M_2(z)$ are reflection matrices from the potential region on the right of z and on the left of z respectively; $M_1(z')$ and $M_2(z')$ are reflection matrices due to the potential region on the right of z' and the left of z' respectively; M^{++} and M^{-+} are transmission and reflection matrices respectively for a right moving incident wave due to the potential slab between z and z'; M^{--} and M^{+-} are transmission and reflection matrices respectively for a left moving incident wave due to the potential slab between z and z'.

constant potential v (see figure 3). It can be proved that the transmission matrix m^{++} and reflection matrix m^{-+} are given by

$$m^{++} = -\frac{4k_z\kappa_z\,\mathrm{e}^{\mathrm{i}\kappa_z h}}{\mathrm{e}^{\mathrm{i}2\kappa_z h}(k_z-\kappa_z)^2-(k_z+\kappa_z)^2} \tag{14}$$

$$m^{-+} = -\frac{(k_z-\kappa_z)^2(\mathrm{e}^{\mathrm{i}2\kappa_z h}-1)}{\mathrm{e}^{\mathrm{i}2\kappa_z h}(k_z-\kappa_z)^2-(k_z+\kappa_z)^2} \tag{15}$$

respectively, where

$$\kappa_z = \sqrt{k_z^2 - v}. \tag{16}$$

As each slice has a constant potential, we obtain by spatial inversion symmetry

$$m^{--} = m^{++} \tag{17}$$

and

$$m^{+-} = m^{-+}. \tag{18}$$

To obtain transmission matrices M^{++} and M^{-+} for a slab, we first assume M^{++} and M^{-+} are known, then add one more slice to the slab (figure 4). Let $\bar{M}^{++}$ and $\bar{M}^{-+}$ be the transmission and reflection matrices for the new slab. It can be proved that $\bar{M}^{++}$ and M^{++} are related by

$$\bar{M}^{++} = M^{++}(1 + m^{+-}M^{-+} + m^{+-}M^{-+}m^{+-}M^{-+} + \cdots)m^{++} \tag{19}$$

or

$$\bar{M}^{++} = \frac{M^{++}m^{++}}{1 - m^{+-}M^{-+}} \tag{20}$$

and the relation between $\bar{M}^{-+}$ and M^{-+} is given by

$$\bar{M}^{-+} = m^{-+} + \frac{m^{++}M^{-+}m^{--}}{1 - m^{+-}M^{-+}}. \tag{21}$$

Starting from the boundary condition at $z = z'$ for which $M^{++} = 1$ and $M^{-+} = 0$, we can obtain M^{++}, M^{-+} for the slab between any z and z' by equations (20) and (21). M^{--} and M^{+-} can be found by

$$M^{--} = M^{++} \tag{22}$$

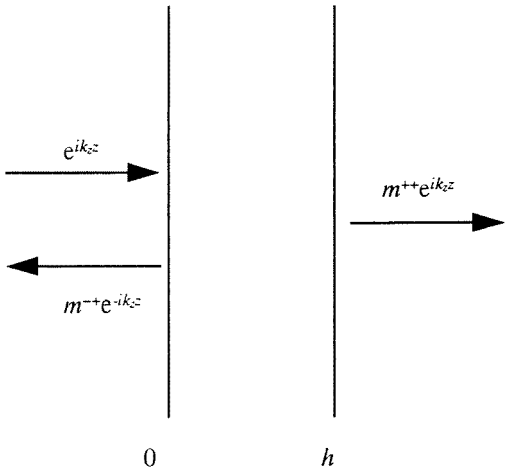

Figure 3. Scattering of a plane wave by a thin slice of constant potential.

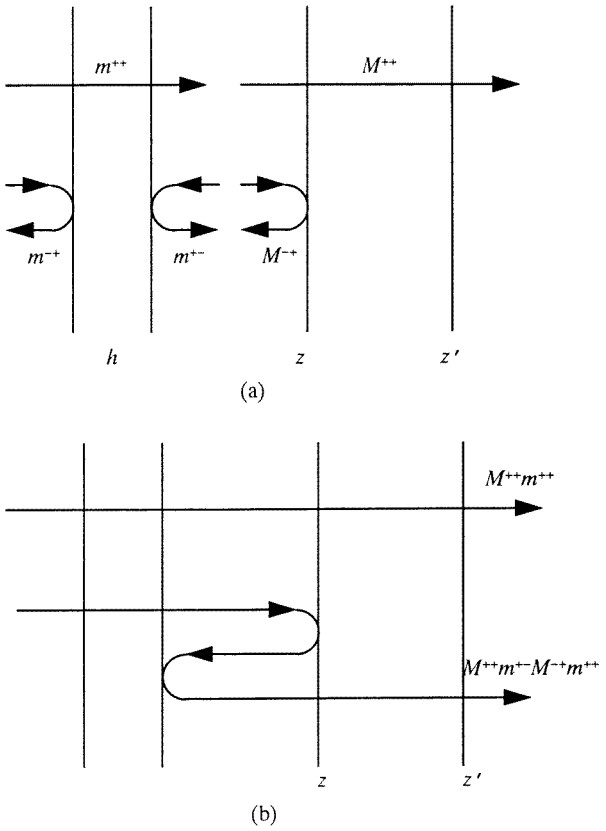

Figure 4. (a) Scattering matrices of a slab and those of a thin slice added on top of the slab. (b) Scattering paths through the system shown in (a).

and

$$M^{+-} = M^{-+}. \tag{23}$$

The calculation of reflection matrices M_1 and M_2 based on the invariant imbedding method is carried out with the same code as the previous work [20]. It is noted that equations (20) and (21) and the equations of M_1 and M_2 are exact as long as the potential of the slice is a constant no matter how large the width h of the slice is. The step size h can be chosen adaptively according to the gradient of the potential in the numerical scheme.

Once the scattering matrices are found, the propagation function can be determined by equations (12) and (13). Substituting equations (12) and (13) into equation (8), we can obtain the Green functions for $z' > z$ and $z' < z$ respectively. The free response function can be calculated by integrating over wavevector $\vec{k}_{\|}$, and summing over the eigenstates below the Fermi energy in equation (7). It is interesting to note that the boundary condition is included in the calculation of the reflection matrices M_1 and M_2, which means that one only has to alter the starting point values of the reflection matrices M_1 and M_2, when the boundary condition is changed. Previous works have shown that the boundary condition has a considerable effect on the collective modes [10]. Various boundary conditions can be readily incorporated in the present method.

Similar to equation (4), the RPA density response function is defined as

$$\delta n_{RPA}(z, q_\parallel, \omega) = \int \mathrm{d}z' \Pi^{RPA}(q_\parallel, z, z', \omega) v(z', q_\parallel). \tag{24}$$

It can be proved that the RPA response function is related to the free response function by the integral equation

$$\Pi^{RPA}(z, z', \vec{q}_\parallel, \omega) = \Pi^0(z, z', \vec{q}_\parallel, \omega) + \iint \mathrm{d}z_1 \, \mathrm{d}z_2 \Pi^0(z, z_1, \vec{q}_\parallel, \omega) v(z_1, z_2) \Pi^{RPA}(z_2, z', \vec{q}_\parallel, \omega) \tag{25}$$

where

$$v(z_1, z_2) = \frac{\partial^2}{\partial n^2}(n\varepsilon_{xc})\delta(z_1 - z_2) + \frac{2\pi}{q_\parallel} \exp(-q_\parallel |z_1 - z_2|) \tag{26}$$

is the function describing the dependence of the potential field on the electron density for a quantum well. ε_{xc} is the exchange–correlation kernel.

In order to simulate spatially nonuniform excitation of a quantum well, the external perturbation potential is chosen to be

$$v_x(z, q_\parallel) = \exp(q_\parallel z). \tag{27}$$

So the strength function can be calculated by

$$M(q_\parallel, \omega) = -\mathrm{Im} \iint \mathrm{d}z \, \mathrm{d}z' \exp(q_\parallel z) \Pi^{RPA}(z, z', q_\parallel, \omega) \exp(q_\parallel z'). \tag{28}$$

This strength function can be directly obtained from experimental measurements. The same function appears in the dipole theory of electron energy loss [22] as well as the theory of infrared (IR) absorption aided by a grating coupler [23, 24].

3. Numerical method

In this section, we will discuss the numerical procedures for the calculation of the excitation spectra of GaAs/$Ga_{1-x}Al_x$As quantum wells based on the invariant imbedding method developed in section 2.

For the calculation of the free response function, we choose the x axis such that k_x is parallel to $\vec{q}_\parallel$. Equation (7) can be rewritten as

$$\Pi^0(q_\parallel, z, z', \omega) = \frac{1}{\pi^2} \sum_i^{occ} \psi_i(z)\psi_i(z') \int_{-k_i}^{k_i} \mathrm{d}k_x \sqrt{k_i^2 - k_x^2} [G^+(z, z', \varepsilon^+) + G^-(z, z', \varepsilon^-)] \tag{29}$$

where

$$k_i = \sqrt{2(\varepsilon_f - \varepsilon_i)} \tag{30}$$

$$\varepsilon^\pm = \varepsilon_i \pm (\omega + k_x q_\parallel) - \tfrac{1}{2} q_\parallel^2. \tag{31}$$

The above function is evaluated on a discrete grid of z and z' points. In order to produce numerically tractable results, a small imaginary part of 0.002 au* (starred Hartree units, see below) has been added to ω, the frequency of the external field, that is $\omega \to \omega + \mathrm{i}\delta$. Since the free response function has a cusp at $z' = z$, the z' integral will be split into two parts at $z' = z$, and the integral over z' is done by Gaussian quadrature. It is noted that although the wave function above the Fermi level spreads far outside the quantum well, especially for the neutral quantum well, the wave functions below the Fermi energy will decrease very quickly to zero outside the quantum well and so does the free response function. In the present work, the

Green functions, sums of the eigenstates both below and above the Fermi energy, are obtained by the invariant imbedding method. Only a few points are taken to sample the region where the wave functions below the Fermi level are almost zero and the self-consistent potential is nearly constant. The integration of the Green function G^+ along the real axis in the k_x plane from $-k_i$ to k_i is deformed into a semicircle in the upper half complex plane. Because the Green functions are much smoother functions of k_x along such a path than along the real axis, only a few points need to be sampled in the integration. In contrast, $G^-(z, z', \varepsilon^*)$ is analytic in the lower half complex plane. Using the basic property of the Green function,

$$G^*(z, z', \varepsilon) = G(z', z, \varepsilon^*) \tag{32}$$

we compute the Green function $G^-(z, z', \varepsilon^-)$ in the same way as $G^+(z, z', \varepsilon^+)$.

Ignoring frequency dependence, the exchange–correlation kernel ε_{xc} in equation (26) is chosen to be the simple Wigner form [25] for both the ground state and the excited state,

$$\varepsilon_{xc} = -\frac{0.458}{r_s} - \frac{0.44}{r_s + 7.8} \tag{33}$$

where

$$r_s \equiv r_s(z) = [\tfrac{4}{3}\pi n(z)]^{-1/3} \tag{34}$$

and $n(z)$ is the self-consistent electron density. The RPA response function is calculated by solving the matrix equation (25).

Previous theoretical works [8–10] indicated that the shape of the quantum well and the boundary condition of the electron gas in the neutral quantum well have a considerable effect on the collective modes in the quantum well of the $Ga_{1-x}Al_xAs$ system. In this work, we will compare the collective modes of neutral quantum wells (NQWs) with those of parabolic quantum wells (PQWs). According to the Poisson equation, we can mimic the bare confining potential $V_{bare}(z)$ of the quantum well due to a varying composition along the z direction as the potential due to the positive charge distribution with density n^+ in a slab [26]. In the calculation, such a fictitious positive charge n^+ is used to parametrize the quantum wells. The width d of the positive charge region in a neutral quantum well is defined as the width of the quantum wells. The approximate width N_S/n^+ that the electrons occupy in a parabolic quantum well is taken to be the width d for the parabolic quantum well. In the present work, we calculate the dynamic response by imposing hard walls at different positions to explore the effects of boundary conditions on the excitation spectra of NQWs.

In our calculation, the effective mass m^* and dielectric constant ϵ are taken to be $m^* = 0.069\ m_0$, and $\epsilon = 12.9$ [27]. For convenience, we use 'starred Hartree units', au*, in which $e^2/\epsilon = 1$, $m^* = 1$, $\hbar = 1$. So 1 au* of length is equal to 102 Å, 1 au* of energy is 11 MeV, which is equivalent to a photon with a reciprocal wavelength of 88.5 cm^{-1}.

4. Results and discussion

Experimental far-infrared transmission spectra of $Ga_{1-x}Al_xAs$ parabolic quantum wells show two strong resonance peaks which can be identified as a 2D-like surface plasmon and a bulklike plasmon [4]. Self-consistent TDLDA and RPA calculations [8–10] on excitation modes of PQW produced excitation spectra whose major peak positions are in good agreement with the experiment. Other theoretical studies were based on the non-retarded, local optics model of a uniform slab of Drude electrons [28]. In this model, the dielectric function within a slab of thickness d is written as

$$\varepsilon = \varepsilon_0(1 - \omega_p^2/\omega^2) \tag{35}$$

where

$$\omega_p^2 = 4\pi n \tag{36}$$

is the bulk plasma frequency. n is the electron density of the slab. Assuming spatially local response and neglecting incoherent scattering, the dispersions of the two plasma modes are given by

$$\omega_\pm^2 = \tfrac{1}{2}\omega_p^2(1 \pm \exp(q_\parallel d)). \tag{37}$$

It was found that equation (37) describes quite well the positions of resonant peaks in the experimental excitation spectra, especially for small wave vector and narrow quantum wells. The low-frequency mode ω_- is attributed to two-dimensional resonant oscillation in the quantum well parallel to the interface (x–y plane), while the high-frequency mode ω_+ is due to transitions between adjacent bound levels in the well corresponding to oscillation of electrons perpendicular to the interface (z direction). They are referred to as intrasubband and intersubband plasmon respectively.

To test the present invariant imbedding scheme, we first consider the PQW. The calculated spectrum $\mathrm{Im}\,[M(q_\parallel, \omega)]$ of a PQW with $n^+ = 0.0275$ au*, $d = 8.8$ au*, $q_\parallel = 0.016$ au* is shown in figure 5. The experimental spectrum of Pinsukanjana *et al* is presented for comparison. It is noted that our results are in good agreement with the experimental data of Pinsukanjana *et al* [4]. In figure 6, we compare the plasmon dispersion relation calculated by the invariant imbedding approach and that obtained from equation (37). Good agreement is found between the two sets of data.

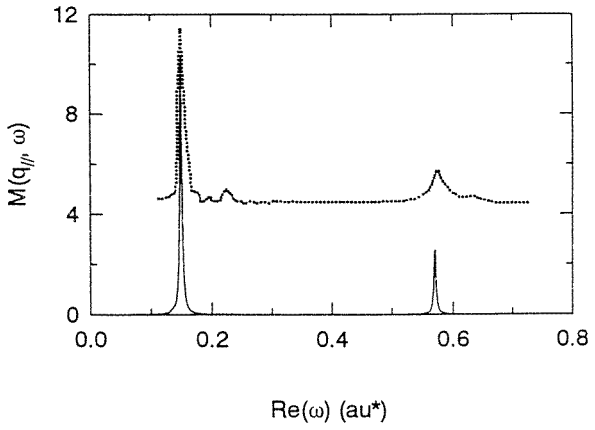

Figure 5. Comparison of excitation spectra obtained in the present study (solid line) and experimental results [4] (dotted line) for a PQW with width $d = 8.8$ au*, density $n^+ = 0.0275$ au*, $q_\parallel = 0.016$ au* and Im $(\omega) = 0.002$ au*.

The excitation spectra are more difficult to interpret for neutral quantum wells (NQWs) [8]. The identification of the resonant peaks on the calculated spectra has so far been ambiguous. For neutral quantum wells, the self-consistent potential energy tends to a plateau value V_p, which is slightly larger than the Fermi energy as $|z| \to \propto$. So the spectrum becomes continuous beyond V_p. Most of the previous calculations were carried out with hard-wall boundary conditions. Two infinite barriers were imposed on both boundaries to make the wave functions vanish at this artificial infinite barrier. Recently, Schaich *et al* calculated the spectrum with a soft-wall boundary condition. They used

$$V(|z| > L_b/2) = V_p \tag{38}$$

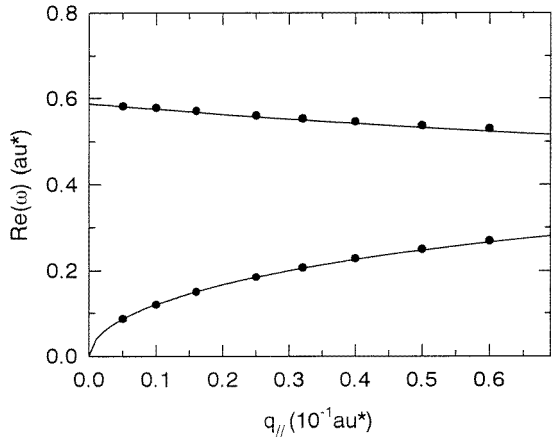

Figure 6. Dispersion relations (dots) of intersubband plasmon modes (upper curve) and intrasubband plasmon modes (lower curve) for a PQW calculated with width $d = 8.8$ au* and density $n^+ = 0.0275$ au*. Solid lines stand for dispersion profiles predicted from the local optical model.

and matched each ψ_n to appropriate analytic solutions outside $\pm L_b/2$, where L_b is the distance between the left and right boundaries used in calculation of the self-consistent ground state. They found that the boundary condition significantly affects the excitation spectra, generally reducing the number of peaks that appear. Such a reduction of resonant peaks is still not fully understood. Since the invariant imbedding approach can readily be adapted to various boundary conditions, it is used here to explore the boundary effects on the excitation spectra of NQWs.

In NQWs, the electrons spread far outside the well. For an NQW with $d = 8.8$ au*, $n^+ = 0.0275$ au*, the width of the self-consistent electron distribution is more than 22 au*, nearly three times the width of the positive background. In the present work, we calculate the ground state electronic structures with width $L_b = 3d$ and $L_b = 4d$ respectively. The calculations show that the ground state density profile with $L_b = 3d$ is almost the same as that with $L_b = 4d$, and the plateau value of the self-consistent potential V_p is 0.575 au* for both cases. This is expected because the boundary condition hardly affects the eigenvalues and eigenfunctions below the Fermi level as long as all the electrons are included in the calculation (i.e. $L_b \geqslant 3d$ in this case). However, it will significantly change the eigenvalues and eigenfunctions above the plateau value of the self-consistent potential and hence affect the dynamic response. To study this effect, we adopt the following strategy. In the case of $L_b = 4d$, the dynamic response is calculated by imposing hard walls at different positions $z_c = \pm L_d/2$ (see figure 1), where $L_d \geqslant 4d$. The potential between $L_b/2$ $(-L_d/2)$ and $L_d/2$ $(-L_b/2)$ is taken to be V_p, the plateau value of the self-consistent potential outside the well. When $L_d \to \infty$, it corresponds to the case of a soft-wall boundary. In figure 7, we present the excitation spectra Im $[M(q_\parallel, \omega)]$ with $L_b = 3d$, $L_d = 3d$ and $q_\parallel = 0.016$ au* for an NQW of $n^+ = 0.0275$ au*, $d = 8.8$ au*. It is found that the number of peaks, the positions and the relative strength of peaks in the response spectrum are in good agreement with those of Schaich and Dobson using the hard-wall boundary condition [10] (the dashed line in figure 7). Since almost the same parameters are used in the two calculations, this again verifies the validity of the present approach. In figure 8, the excitation spectra Im $[M(q_\parallel, \omega)]$ are shown for $n^+ = 0.0275$ au*, $d = 8.8$ au* and $q_\parallel = 0.016$ au* under different boundary conditions.

In figure 8(a), we show the excitation spectrum with $L_b = 3d$, $L_d = 3d$. Figures 8(b)–(d) show the excitation spectra with $L_b = 4d$, and $L_d = 4d$, $8d$, $12d$ respectively. It is noted in our calculation that there is a sudden change in the positions and relative amplitudes of most peaks in the excitation spectra when L_d is increased from $3d$ to $4d$. According to figure 8(b), a very sharp peak at $\omega = 0.56$ au* appears instead of peaks HPt and TB3 in figure 8(a), which are close to the bulk plasmon frequency. Two very close peaks appear instead of the peaks TB2 and MPt. We note that in figure 8(b) peak TB4 and the small peaks T1, T2 are located at almost the same positions as in figure 8(a). The peak TB1, at $\omega = 0.268$ au*, vanishes, and a new small peak TB5, at $\omega = 0.34$ au*, appears. When L_d is increased, peaks T1 and T2 gradually grow and some weak resonances appear and vanish again. When we move the hard wall to $L_d = 12d$ in figure 8(d), the calculated spectrum yields three stable and strong peaks T2, MP, HP in the frequency region from 0.35 au* to the bulk plasmon frequency. They are at frequencies 0.385, 0.470 and 0.570 au* respectively, which correspond to the three peaks in the excitation spectrum with the soft-wall boundary [10]. The three peaks LP, T1, T2 in figure 8(d) correspond to LP, T1, T2 in figure 8(a). However it is difficult to find the corresponding peaks in figure 8(a) for the two peaks MP, HP in figure 8(d). It is noted that the peaks in figure 8(d) with a hard-wall boundary condition of $L_d = 12d$ are much sharper than those with soft-wall boundaries [10]. We expect that if L_d is increased further, the peaks will broaden and resemble those calculated with the soft-wall boundaries.

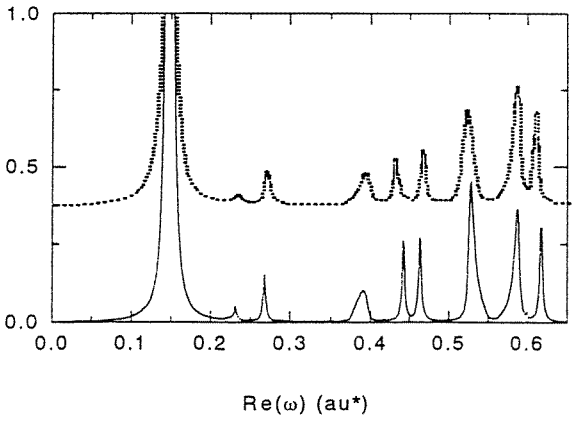

Figure 7. Comparison of excitation spectra (solid curve) for an NQW with $d = 8.8$ au*, density $n^+ = 0.0275$ au*, $q_\parallel = 0.016$ au* under hard-wall boundary conditions $L_b = L_d = 3d$ with those (dotted curve) calculated by Schaich and Dobson under similar conditions [10].

To understand the origin of the resonances, we calculate the induced electron density, which is defined as

$$\delta n \equiv \delta n_{RPA}(\omega, z) = -\mathrm{Im} \int \mathrm{d}z' \, \Pi^{RPA}(z, z', \omega) \exp(q_\parallel z'). \tag{39}$$

Consider first the excitation spectrum shown in figure 8(d). The frequency and the induced density of the strongest peak LP are similar to those of the PQW, so it is readily identified as the intrasubband plasmon. That its position is independent of the boundary conditions also confirms the identification. The resonance HP has been identified with ω^+, the intersubband plasmon mode [8–10]. The position and the induced density profiles in our calculation also support this identification. Schaich and Dobson [10] attributed peak MP to both the multipole plasma mode and intersubband transition resonance. In our calculation, the peak

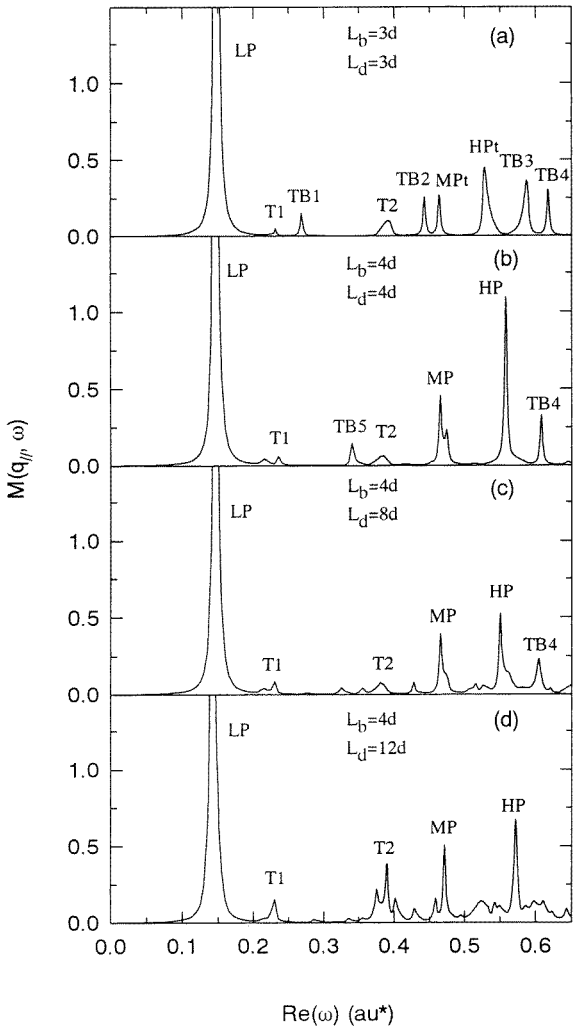

Figure 8. Comparison of the excitation spectra for an NQW with $d = 8.8$ au*, density $n^+ = 0.0275$ au*, $q_\parallel = 0.016$ au* under different boundary conditions: (a) $L_d = 3d$, (b) $L_d = 4d$, (c) $L_d = 8d$, (d) $L_d = 12d$. The self-consistent electron structures are calculated with $L_b = 3d$ for (a), $L_b = 4d$ for (b), (c), (d). The intrasubband plasmon modes (low-frequency modes) are labelled as LP. The intersubband plasmon modes (high-frequency modes) are labelled as HP. The multipole plasmon modes are labelled as MP. T1 and T2 represent the intersubband transition resonances whose frequencies are independent of the boundary conditions, while TB1, TB2, TB3, TB4, TB5 stand for the intersubband transition modes whose positions depend on the boundary conditions.

MP demonstrates the characteristics of the multipole plasma mode, which is usually observed on simple metal surfaces [29–32]. Firstly, the frequency is about 0.8 ω_p. Secondly, the induced density profile is odd in z and the integrals of the induced density with respect to each surface are nearly zero. So this resonance can be identified as a collective multipole plasma mode rather than an intersubband transition. The peaks T1 and T2 can be identified as the intersubband transitions from the third subband to the fifth subband and from the third subband to the fourth subband respectively [10]. We find that the corresponding induced density profiles

in our calculation, shown in figure 9, are nearly identical to those of Schaich and Dobson [10]. The energies of the third, fourth and fifth subbands are hardly altered when we increase L_d because they are below the plateau value of the self-consistent potential V_p. So the fact that the positions of the peaks T1, T2 are almost independent of the boundary conditions confirms the above identification of peaks T1 and T2.

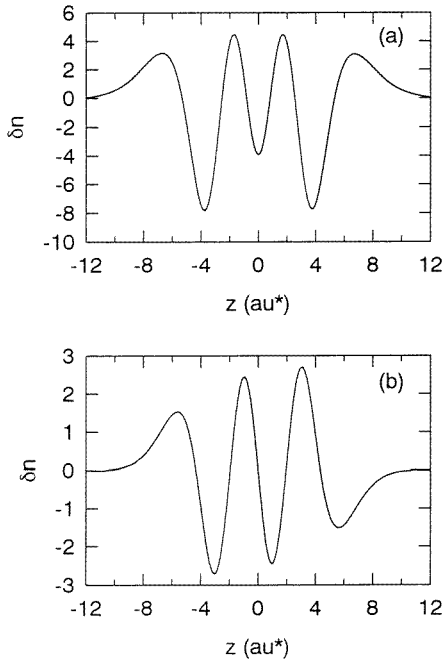

Figure 9. Induced density profiles corresponding to peaks (a) T1, $\omega = 0.23$ au* and (b) T2, $\omega = 0.391$ au* in the excitation spectra of figure 8(a).

In what follows, we will consider the origins of the remaining peaks in figure 8(a). Shown in figures 10(a)–(c) are the induced densities of TB1, TB2 and TB3 respectively. They can be identified as the intersubband transitions of third to sixth, third to eighth, and second to seventh subbands respectively by comparing their induced density profiles with the single-particle estimates, which are generated from the product

$$\delta n_{ij} = \psi_i(z)\psi_j(z) \tag{40}$$

for transition from the initial state i to the final state j. The expression is what appears in the first order perturbation theory. At resonance, the contribution of one transition should dominate. The strong dependence of these peaks on the boundary conditions supports the identification because their final states are all above V_p.

In order to understand the evolution of some of the resonant peaks, we propose the following physical picture of the resonant coupling of the plasmon modes and the intersubband transitions. When the frequency of a plasmon crosses that of the intersubband transition, the plasma mode and the intersubband transition mode will interact with each other, and then will split into two neighbouring peaks, with the weak resonance being enlarged. There have been previous investigations on the coupling between different kinds of excitation modes [5, 6, 33–37]. The resonant interaction of intrasubband plasmon and intersubband plasmon was first calculated by Das Sarma [33] using an RPA in a two-band model, and later by Li

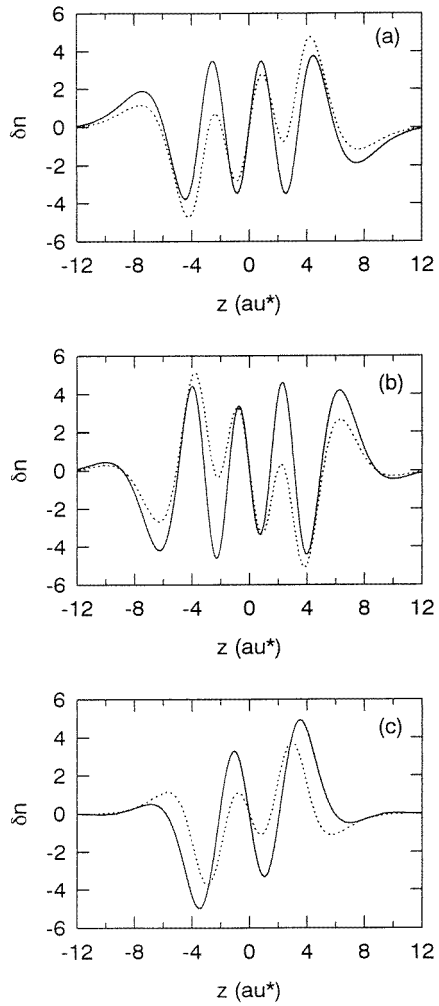

Figure 10. Induced density profiles (solid line) corresponding to peaks (a) TB1, $\omega = 0.268$ au*, (b) TB2, $\omega = 0.442$ au*, (c) TB3, $\omega = 0.587$ au* in the excitation spectra of figure 8(a). The dashed lines represent single-particle estimates based on equation (40): (a) $(i, j) = (3, 6)$, $\Delta\varepsilon_{36} = 0.287$ au*, (b) $(i, j) = (3, 8)$, $\Delta\varepsilon_{38} = 0.0478$ au*, (c) $(i, j) = (2, 7)$, $\Delta\varepsilon_{27} = 0.537$ au*.

and Das Sarma [34], and by Gold and Ghazali [35]. Experimentally, such coupling has been observed by Oelting *et al* [36] in a two-dimensional electron system on silicon–MOS structures by tuning their energies via uniaxial stress. Recently it was observed in a parabolically confined electron system by Kaloudis *et al* [5]. The coupling of the intersubband plasma mode and inter-Landau transition was studied by Liao *et al* [6]. The influence of the collective excitation on the intersubband transition energies has been observed in the determination of the specific single-particle energies in the inversion electrons in GaAs in optical experiments [37, 38]. However, to the best of our knowledge, there has been no report on theoretical or experimental study on the strong coupling of collective modes and intersubband transitions. In figure 8, when we decrease the distance between the hard walls from $L_d = 12d$ to $L_d = 8d$, two new intersubband transitions appear close to the multipole plasmon MP and intersubband plasmon

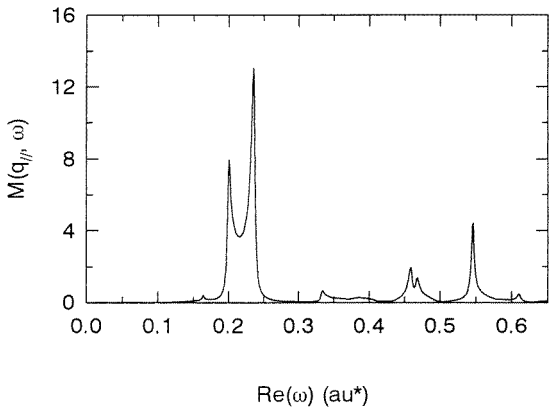

Figure 11. Excitation spectrum for an NQW with width $d = 8.8$ au*, density $n^+ = 0.0275$ au*, $q_\parallel = 0.040$ au* and Im $(\omega) = 0.002$ au*.

HP respectively, which result in slight shifts in position and decreases in amplitude of both peaks MP and HP. When $L_d = 4d$, the peak near peak HP disappears and the amplitude of peak HP increases, while the peak near MP starts to split. When L_d is further decreased, the peak HP splits into two widely separated peaks HPt and TB3, while MP and the peak nearby are split into distinct peaks MPt and TB2. From figure 8(a)–(d), as L_d is varied, the amplitudes of peaks MP and HP decrease when they are approached by neighbouring peaks and increase again when the neighbouring peaks move away. So we may associate the peaks MPt and HPt with collective modes MP and HP respectively. The induced densities also confirm the association. The small peaks that emerge in $L_d = 8d$ are related to intersubband transitions TB2 and TB3 respectively. As discussed above, the variation of L_d will change the final state energies of TB2 and TB3, which are both above V_p. This in turn will alter their intersubband transition frequencies. From $L_d = 4d$ to $L_d = 12d$, the intersubband transitions TB2 and TB3 have little effect on the positions and amplitudes of the collective modes MP and HP because their resonant frequencies are not sufficiently close to those of the collective modes. When L_d is decreased to $3d$, the frequencies of the two intersubband transitions cross those of the plasmon modes MP and HP respectively. As a consequence, a strong resonant interaction of plasmon modes and intersubband transitions gives rise to the large shift of resonance frequencies and the enhancements of the resonances. So the calculated spectra show all the characteristics of a resonant interaction, i.e. a resonant enhancement of the intersubband resonant amplitude and a splitting of the dispersion. Similar to some previous works [6–8], we have identified three plasma modes in the neutral quantum well, i.e. intrasubband plasma mode, multipole plasma mode and intersubband plasma mode respectively. We have observed the resonant coupling of the multipole plasmon and intersubband plasmon with the intersubband transitions. As for the intrasubband plasmon, there is a very weak nearby intersubband transition resonant peak, T1. However there is no interaction between them because their frequencies are 0.08 au* apart. It is well known that the intrasubband plasmon has a large positive dispersion [28]. We will consider what happens when its frequency crosses that of the peak T1 by increasing the wavevector. Shown in figure 11 is the calculated excitation spectrum for the same quantum well with $q_\parallel = 0.040$ au*. The results are just as expected. A strong resonant coupling between the intrasubband plasmon and intersubband transition resonance T1 results in a shift of resonant frequencies and strong enhancement of the intersubband transition. Taking this picture into account, we can explain the physical causes of all the resonant peaks in the excitation spectra.

The resonant peaks can be classified into two groups. One group is due to collective resonance, which are intrasubband plasma mode LP, multipole plasma mode MP and intersubband plasma mode HP respectively. The other group is due to the intersubband transition. The frequencies of these resonant peaks are almost independent of the boundary condition if their final states are below V_p, the plateau value of the self-consistent potential outside the well. However, these resonant modes are not stable and their resonant frequencies depend on the boundary conditions if their final states are above V_p. In the case when these two types of excitation mode cross each other, a resonant coupling gives rise to an enlargement of the intersubband transition amplitude and shifts in the resonance frequencies.

5. Concluding remarks

An alternative approach based on the invariant imbedding method is used to study the excitation spectra of both the NQW and PQW. Compared to other approaches, the present method is more efficient and leads to more stable solutions. The boundary conditions are naturally incorporated in the calculation, and therefore it provides a convenient way for studying boundary effects. The calculated results for both the NQW and PQW are in good agreement with available experimental data and results of previous calculations. It was found that the positions of resonant peaks on the spectra of the NQW are sensitive to the boundary condition. Evolution of the resonant peaks was shown to be due to coupling between collective plasma modes and intersubband transitions. The observed resonant peaks of the NQW have been classified according to their physical origins and the dependence of their properties on the boundary condition.

It is interesting to note that when the barrier (AlAs) width and height of an InGaAs/AlAs/InAs resonant tunnelling diode grown on an ZnP substrate by MBE [14] are sufficiently large, the system will behave like a quantum well with hard-wall boundaries. The position of the wall can be adjusted by varying the width of the InGaAs layer. According to the present work, the resonant coupling between collective plasma modes and intersubband transition modes can be studied in such a system with the appropriate boundary conditions.

References

[1] Sundaram M, Gossard A C, English J H and Westervelt R M 1988 *Superlatt. Microstruct.* **4** 683
[2] Shayegan M, Sajoto T, Santos M and Silvestre C 1988 *Appl. Phys. Lett.* **53** 791
[3] Wixforth A, Sundaram M, Ensslin K, English J H and Gossard A C 1991 *Phys. Rev.* B **43** 10 000
[4] Pinsukanjana P R, Gwinn E G, Dobson J F, Yuh E L, Asmar N G, Sundaram M and Gossard A C 1992 *Phys. Rev.* B **46** 7284
[5] Kaloudis M, Ensslin K, Wixforth A, Sundaram M, English J H and Gossard A C 1992 *Phys. Rev.* B **46** 12 469
[6] Liao L B, Heiman D, Hopkins P F and Gossard A C 1994 *Phys. Rev.* B **49** 16 825
[7] Brey L, Johnson N F and Halperin B I 1989 *Phys. Rev.* B **40** 10 647
Brey L, Dempsey J, Johnson N F and Halperin B I 1990 *Phys. Rev.* B **42** 1240
[8] Dobson J F 1992 *Phys. Rev.* B **46** 10 163
[9] Dobson J 1993 *Aust. J. Phys.* **46** 391
[10] Schaich W L and Dobson J F 1994 *Phys. Rev.* B **49** 14 700
[11] Ritchie R H 1957 *Phys. Rev.* **106** 874
[12] Yuh E L, Gwinn E G, Pinsukanjana P R, Schaich W L, Hopkins P F and Gossard A C 1993 *Phys. Rev. Lett.* **71** 2126
[13] Heinonen O and Kohn W 1993 *Phys. Rev.* B **48** 12 240
[14] Broekaert T P E, Lee Wai and Fonstad C G 1988 *Appl. Phys. Lett.* **53** 1545
[15] Eguiluz A G 1985 *Phys. Rev.* B **31** 3303
[16] Gies P, Gerhardts R R and Maniv T 1987 *Phys. Rev.* B **35** 458
[17] Feibelman P J 1982 *Prog. Surf. Sci.* **12** 287

[18] Guo Q, Feng Y P, Poon H C and Ong C K *Eur. Phys. J.* B at press
[19] Poon H C and Howe P T 1992 *Mod. Phys. Lett.* **4** 459
[20] Secrest D 1979 *Atom–Molecule Collision Theory* ed R B Bernstein (New York: Plenum)
Light J C and Walker R B 1976 *J. Chem. Phys.* **65** 4272
[21] Zhao T C, Poon H C and Tong S Y 1988 *Phys. Rev.* B **38** 1172
[22] Mills D L 1975 *Surf. Sci.* **48** 59
[23] Zheng Lian, Schaich W L and MacDonald A H 1990 *Phys. Rev.* B **41** 8493
[24] Schaich W L, Park P W and MacDonald A H 1992 *Phys. Rev.* B **46** 12 643
[25] Mahan D 1989 *Many Particle Physics* (New York: Plenum) p 405
[26] Burt M G 1992 *J. Phys.: Condens. Matter* **4** 6651
[27] Adach S (ed) *Properties of Aluminium Gallium Arsenide* (London: Inspec)
[28] Raether H 1988 *Surface Plasmons on Smooth and Rough Surfaces and on Gratings* (Berlin: Springer)
[29] Kempa K, Liebsch A and Schaich W L 1988 *Phys. Rev.* B **38** 12 645
[30] Dobson J F and Harris G H 1988 *J. Phys. C: Solid State Phys.* **21** L729
Dobson J F, Harris G H and O'Connor A J 1990 *J. Phys.: Condens. Matter* **2** 6461
[31] Tsuei K-D, Plummer E W, Liebsch A, Kempa K and Bakshi P 1990 *Phys. Rev. Lett.* **64** 44
[32] Quinn J J 1992 *Solid State Commun.* **84** 139
[33] Das Sarma S 1984 *Phys. Rev.* B **29** 2334
[34] Li Q and Das Sarma S 1989 *Phys. Rev.* B **40** 5680
[35] Gold A and Ghazali A 1990 *Phys. Rev.* B **41** 8318
[36] Oelting S, Heitmann D and Kotthaus J P 1986 *Phys. Rev. Lett.* **56** 1846
[37] Ando T, Fowler A B and Stern F 1982 *Rev. Mod. Phys.* **54** 437
[38] Batke E 1991 *Adv. Solid State Phys.* **31** 297